HHS Public Access

Author manuscript

Nat Struct Mol Biol. Author manuscript; available in PMC 2013 March 01.

Published in final edited form as:

Nat Struct Mol Biol. 2012 September ; 19(9): 906–915. doi:10.1038/nsmb.2366.

Nectin ectodomain structures reveal a canonical adhesive interface

Oliver J. Harrison[1,2,3], **Jeremie Vendome**[1,2,3], **Julia Brasch**[1,3], **Xiangshu Jin**[1,2,3], **Soonjin Hong**[4], **Phinikoula S. Katsamba**[1,2,3], **Goran Ahlsen**[1,2,3], **Regina B. Troyanovsky**[4], **Sergey M. Troyanovsky**[4], **Barry Honig**[1,2,3,*], and **Lawrence Shapiro**[1,3,*]

[1]Department of Biochemistry and Molecular Biophysics, Columbia University, 1150 Saint Nicholas Avenue, New York, NY 10032, USA

[2]Howard Hughes Medical Institute, Columbia University, 1130 Saint Nicholas Avenue, New York, NY 10032, USA

[3]Columbia Initiative in Systems Biology, Columbia University, 1130 Saint Nicholas Avenue, New York, NY 10032, USA

[4]Department of Dermatology, Northwestern University, The Feinberg School of Medicine, Chicago, IL, USA

Abstract

Nectins are immunoglobulin superfamily glycoproteins that mediate intercellular adhesion in many vertebrate tissues. Homophilic and heterophilic interactions between nectin family members help to mediate tissue patterning. We determined homophilic binding affinities and heterophilic specificities of all four nectins and the related protein nectin-like 5 from human and mouse, revealing a range of homophilic strengths and a defined heterophilic specificity pattern. To understand the molecular basis of adhesion and specificity, we determined crystal structures of natively glycosylated full ectodomains or adhesive fragments of nectins 1–4 and nectin-like 5. All crystal structures reveal dimeric nectins bound through a stereotyped interface previously proposed to represent a *cis* dimer. However, conservation of this interface and results of targeted cross-linking experiments show that this dimer likely represents the adhesive *trans* interaction. Its structure provides a simple molecular explanation for the adhesive binding specificity of nectins.

Correspondence should be addressed to B.H. (bh6@columbia.edu) and L.S. (lss8@columbia.edu).

Accession codes. Protein Data Bank: Coordinates for human nectin-1 D1-3, mouse nectin-2 D1-2 crystal forms 1 and 2, human nectin-3 D1-3, human nectin-4 D1-2, human Necl-5 D1-3 and mouse F136D mutant nectin-2 D1-2 have been deposited with accession codes 4FMF, 4FMK, 4FNO, 4FOM, 4FRW, 4FQP and 4FS0, respectively.

AUTHOR CONTRIBUTIONS

O.J.H, J.B. and X.J. determined and refined all crystal structures; O.J.H. produced all wild-type and mutant proteins; P.S.K. performed and analyzed the SPR experiments; G.A. performed and analyzed the AUC experiments, J.V. performed all bioinformatic analyses; S.H., R.B.T. and S.M.T performed immunofluorescence and cross-linking studies; O.J.H., B.H. and L.S. designed experiments, analyzed data and wrote the manuscript.

INTRODUCTION

Nectins comprise a small family of immunoglobulin (Ig) superfamily cell adhesion proteins containing four members, nectins 1–4 (also known as poliovirus receptor-related proteins 1–4), that are conserved in vertebrate species[1–4]. Nectins are characterized by an ectodomain containing three tandem Ig-like regions arranged as an N-terminal variable-like domain (D1) followed by two constant-like domains (D2-3), a single transmembrane region and a cytoplasmic domain that binds to the actin cytoskeleton through the adaptor protein afadin[5]. Alternative splicing gives rise to additional splice forms of nectins 1, 2 and 3, which differ in their transmembrane and cytoplasmic regions[3]. A highly related family of proteins, referred to as nectin-like (Necl) proteins 1–5, share a similar domain organization, but do not bind to afadin. Of these, Necl-1-4 are highly similar to each other and are likely to represent a functionally distinct subfamily, also referred to as synaptic cell adhesion molecules (synCAMs)[6]. Necl-5 (also known as poliovirus receptor), while also unable to bind afadin, is more closely related to nectins at the sequence level[6, 7]. The present study focuses on the nectin subfamily and the highly related protein Necl-5.

Nectins mediate calcium-independent cell-cell adhesion in many vertebrate tissues including epithelia, endothelia and neural tissue during development and in adulthood[3, 8, 9]. Individual nectin subtypes are expressed in distinct, but overlapping patterns such that a given cell may express one or a combination of several nectins[10]. At the subcellular level, nectins are restricted to subapical regions of lateral membranes in polarized epithelial cells, where their localization appears to overlap with that of *zonula adherens* components including cadherins[11–13]. Nectins 1–4 each mediate homophilic cell adhesion (i.e. between cells expressing identical nectin subtypes) and have been shown to drive cell aggregation when exogenously expressed in normally non-adherent cells[11, 12, 14, 15] and to localize symmetrically at homotypic cell-cell contacts[16–18]. Additionally, nectins engage in heterophilic adhesion in specific pairwise combinations: heterophilic adhesion has been observed between nectin-1 and nectin-3; nectin-1 and nectin-4; and between nectin-2 and nectin-3 in mixed cell aggregation assays, co-culture experiments [10, 12, 19, 20], and in binding assays using purified proteins[7, 17, 21, 22]. Notably, heterophilic interactions appear to be markedly stronger than the respective homophilic interactions in these assays, resulting in larger cell aggregates[20], higher resistance to separation force[23] or higher levels of protein binding[17, 21]. Necl-5, unlike nectins 1–4, does not mediate homophilic aggregation of transfected cells[7, 14], but weakly binds heterophilically to nectin-3[7, 21, 24].

Heterophilic binding between cognate nectin pairs that is stronger than homophilic binding of either subtype appears to underlie a unique role for nectins in mediating heterotypic cell-cell association[10]. Mice genetically null for individual nectins are viable and develop to adulthood, likely due to redundancy between nectin subtypes in most tissues[10, 25–27], but display developmental phenotypes that reveal non-redundant roles for their heterophilic interactions. Nectin-1 (*Pvrl1*$^{-/-}$) and nectin-3 (*Pvrl3*$^{-/-}$) knockout mice both display micropthalmia resulting from phenotypically identical defects in formation of the ciliary body of the eye where heterophilic binding between nectin-1 and nectin-3 is required to link two distinct epithelial layers[26]. Nectin-2 (*Pvrl2*$^{-/-}$) and nectin-3 (*Pvrl3*$^{-/-}$) knockout mice show male-specific infertility due to defects in sperm development, for which heterophilic

adhesion between nectin-2 expressed in the seminiferous epithelium and nectin-3 in developing spermatids appears to be a crucial[25, 28]. In human disease, mutations in the genes encoding nectin-1 and nectin-4 are associated with cleft lip/palate-ectodermal dysplasia and ectodermal dysplasia-syndactyly syndrome, respectively. These diseases share several common symptoms, suggesting an important role for nectin-1-nectin-4 heterophilic interactions in ectoderm[29, 30].

Homophilic and heterophilic binding between nectins measured in cell aggregation assays[22, 31] and in binding assays using purified proteins[17, 21] critically requires the membrane-distal Ig-variable-like domain, D1, whereas constant-like domains D2 and D3 appear to be dispensable for binding. A recent crystal structure of the ectodomain of human nectin-1, expressed in bacteria, revealed a homodimer formed through the FGCC′C″ sheets of partner D1 domains[20]. Mutations targeting hydrogen bonding residues in the interface were shown to abrogate homophilic and heterophilic adhesion and to inhibit homodimerization of the purified protein in solution[20]. However, the authors concluded that the crystallographic dimer represented a *cis* dimer (between nectins on the same cell) rather than a *trans* dimer (between nectins on apposed cells), in part because the orientation of the interacting protomers was compatible with either a *cis* or *trans* dimer and in part because mutation of the interface, in addition to abolishing adhesion, also diminished the proportion of nectin that could be chemically cross-linked as dimer on the surface of dissociated transfected cells[20]. Such cross-linking assays have been cited as evidence for nectin *cis*-dimerization, since cells are dissociated and no *trans* bonds should form[12, 15, 19, 24]. Based on these data, Narita and colleagues proposed a model for nectin adhesion in which nectins form *cis* dimers on the cell surface through the FGCC′C″ interface that are essential for subsequent *trans* binding through an interface that was not present in the crystals[20]. Since no candidate *trans* binding interface was identified, the structural basis for nectin adhesion, and consequently for nectin adhesive specificity, has remained unresolved.

We undertook a biophysical and structural analysis of the nectin family (nectins 1–4 and Necl-5) in order to determine the molecular basis of nectin adhesion and specificity. Binding between purified nectin ectodomains was tested in all pairwise combinations and equilibrium constants for nectin homodimers were determined. Crystal structures of ectodomains of nectins 1, 2, 3, 4, and Necl-5 presented here identify a single conserved interface that we show, contrary to its previously suggested role as a *cis* dimer, to be the adhesive *trans* interface of nectins. Identification of the nectin adhesive interface provides a framework for understanding the structural basis of nectin adhesive binding specificity, which appears to be mediated in large part by electrostatic compatibility between cognate pairs.

RESULTS

Nectin ectodomains form homophilic and heterophilic dimers

We purified full length, natively glycosylated ectodomains (D1-D3) of human and mouse nectin-1, nectin-2, nectin-3 and nectin-4 and human Necl-5 from conditioned media of transfected human embryonic kidney (HEK) 293 cells. We assessed the homophilic binding properties of the proteins in solution using equilibrium analytical ultracentrifugation (AUC).

Nectins 1–4 from human each showed monomer-dimer equilibrium in solution, with apparent molecular weights in AUC higher than molecular weights of the monomers as determined by mass spectrometry (Table 1). Fitting of the data to a 1:1 binding model yielded dissociation constants ($K_{D)}$ for homodimerization that were in the micromolar range, but varied widely between subtypes. The nectins appeared to fall into two groups: nectin-1 and nectin-2 formed relatively stronger homophilic dimers (K_D 17.5μM and 0.4μM), whereas dimerization of nectin-3 and nectin-4 was very weak(K_D values in the hundred micromolar range). These relative affinities were conserved in mouse nectins 1–4 (64–97% sequence identity to the human orthologs in D1 domains), with tighter homophilic binding for nectin-1 and nectin-2 than for nectin-3 and nectin-4 (Table 1). Necl-5 did not dimerize detectably in solution, consistent with previous reports that it cannot mediate homophilic cell-cell adhesion[7, 14].

We used surface plasmon resonance (SPR) to test heterophilic binding between ectodomains of human nectins 1–4 and Necl-5 in all pairwise combinations (Fig. 1). Specific heterophilic binding was detected between nectin-1 and nectin-3 (Fig. 1a, c), nectin-1 and nectin-4 (Fig. 1a, d), and between nectin-2 and nectin-3 (Fig. 1b and c). Additionally, a very low level of binding was detected between Necl-5 and both nectin-3 and nectin-1 (Fig. 1c and e). Other combinations of nectin subtypes yielded no detectable binding responses. The heterophilic interactions detected in our analyses are in agreement with the results of previous in vitro binding assays[7, 17, 21, 22] and, given that all combinations were tested under comparable conditions, confirm that these specific binding interactions represent the only strong heterophilic pairs in the nectin family. Notably, SPR responses observed for heterophilic binding were higher in all cases than those for homophilic binding at comparable protein levels, with homodimerization detectable only at the highest concentrations tested (Fig. 1 and Supp. Fig, 1). Quantitative kinetic and equilibrium analyses of SPR binding curves were attempted to determine heterophilic nectin binding affinities, but poor fitting of the data was observed, suggesting the method to be unsuitable for determination of binding constants for these proteins (data not shown). Similar problems have been observed with other proteins that self-associate and are likely due to homodimerization of nectins within the immobilized and mobile phases competing with the measured binding interactions[32, 33]. Nonetheless, our semi-quantitative data are consistent with previous studies showing heterophilic binding to be generally favored over homophilic binding.

To determine the stoichiometry of nectin heterophilic interactions in solution, we performed equilibrium AUC analysis on a 1:1 mixture of human nectin-1 and nectin-3. Nectin monomers, homodimers and heterodimers are expected to be at equilibrium in the mixture and the high affinity of the nectin-1-nectin-3 heterophilic interaction should result in an average apparent molecular mass in AUC that approaches the actual molecular mass of the complex. Our analysis yielded an apparent molecular mass of 86.7kDa, corresponding closely to the molecular mass of a hypothetical heterodimer (Table 1) and suggestive of a 1:1 binding stoichiometry. Analysis of a nectin-1-nectin-4 mixture yielded similar results (Table 1). Together, our AUC and SPR data show that purified nectin ectodomains in solution form homophilic and heterophilic dimers with a pattern of activity and specificity that is consistent with adhesive binding behavior observed in cellular studies[10, 12, 19, 20].

Homodimer structures of nectins 1–4 and Necl-5

The overall structure of the nectin extracellular region was revealed in a recent structural study of a bacterially expressed, non-glycosylated full ectodomain region of nectin-1[20]. These researchers identified a dimer interface between partner D1 domains which they interpreted to represent a *cis* dimer putatively formed between nectins emanating from the same cell surface, but no candidate *trans* interface was identified. To help identify the *trans* adhesive interface, we determined crystal structures of full ectodomains or adhesive fragments of human nectin-1 (D1-3), mouse nectin-2 (D1-2, two crystals forms), human nectin-3 (D1-3), human nectin-4 (D1-2) and human nectin-like 5 (D1-3). Crystallographic statistics are summarized in Table 2. Each of these proteins has similar overall structure, with an approximately linear arrangement of tandem Ig-like domains, and all structures except nectin-4 reveal N-linked glycosylation sites added in mammalian processing that are distributed among the D1, D2 and D3 domains with no single glycan site conserved in all family members (Fig. 2).

For each nectin structure we observe a stereotyped homodimer arrangement between the membrane-distal D1 domains (Fig. 2, Table 2). This dimer is the same that was identified by Narita and colleagues[20] as representing a *cis* interface. However, we provide evidence below that this dimer corresponds to the nectin adhesive interface, and its structural details should hence shed light on the adhesive binding specificities of nectins. In each crystal structure the nectin dimer is exactly or approximately 2-fold symmetric, with the majority of inter-protomer contacts centered near the membrane-distal apex of D1. Like other Ig variable-like domains, D1 is formed by two β-sheets formed by the ABED and CC′C″ FG strands (Fig. 3a). The nectin dimer is formed by symmetrical interactions between the CC′C″ FG sheets of two partner D1 domains. The 2-fold dimer axis bisects the dimer mid-way through the paired partner C strands, which form the center of the dimer interface. The F and G strands interact primarily via a substructure containing the FG loop at the apex of D1 that interacts with a pocket formed by the C′ and C″ strands of the partner molecule. The homodimers of nectins 1, 2, 3, 4, and Necl-5 bury 1699Å^2, 1675Å^2, 1341Å^2, 1341Å^2, and 1254Å^2 total interfacial surface area (polar and hydrophobic), respectively, and are stabilized by a combination of hydrophobic contacts, hydrogen bonds, and salt bridges.

Some characteristic interactions are conserved in the dimer interfaces of all five nectin structures. These include intercalation of a Phe in the FG loop (Phe129, 136, 153, 132, and 128 in nectins 1, 2, 3, 4 and Necl5, respectively), into a hydrophobic pocket formed by the C′ and C″ strands of the partner molecule (Fig. 3b). The Phe-acceptor pocket is characterized by a conserved Gly (Gly86, 85, 110, 87 and 83 in nectins 1, 2, 3, 4 and Necl-5) whose α-carbon forms the base of the pocket, accommodating the Phe aromatic ring. Residues flanking this glycine residue have hydrophobic or partial hydrophobic character, as do the adjacent residues on the C′ strand which complete the pocket structure. Notably, the residue preceding the conserved glycine (Met85, Phe84, Tyr109, Tyr86 and Gln82 in nectins 1, 2, 3, 4 and Necl-5) has hydrophobic or partially hydrophobic character in nectins 1–4 and forms the ‘cap’ of the Phe acceptor pocket and interacts closely with the Phe side chain. The sequence in the FG loop around the docking Phe is highly conserved in the motif TFPxG (Supp. Fig. 2). This region folds into a classical type I β-turn with the Pro residue preceding

the turn and Gly at the apex. Other than Phe, other side chains in the TFPxG motif do not make extensive interactions with the partner molecule, suggesting they might function to stabilize the conformation in which the docking Phe is presented. Polar interactions in the dimer interface are not strictly conserved between nectins, but conserved polar residues in the C and C′ strands are involved in symmetrical hydrogen bonding in the center of each interface (Thr83, Gln84 and Asn82 in nectin-1, Fig. 3b, Supp. Fig. 2, Supp. Fig. 3).

Remarkably, in nectins 1–4, a charged residue in the F-strand is positioned in the middle of each homodimer interface (Glu125, Glu132, Lys149, Arg128, in nectins 1, 2, 3, and 4, respectively, Fig. 3b), facing its symmetry-related residue in the partner molecule. This would be expected to result in electrostatic repulsion, potentially destabilizing the interface. That nectins 1–4 bind through this interface indicates that other favorable interactions (see above) outweigh this repulsion. Necl-5 has a hydrophobic amino acid, Leu124, at this position, distinguishing it from classical nectins.

We tested the importance of the structurally observed dimer interface for binding between nectin ectodomain fragments in solution using an F129D mutant of nectin-1 that contained a substitution of the conserved residue Phe129 with Asp to disrupt the interface by introduction of an unpaired negative charge. Equilibrium AUC analysis of the mutant protein revealed homodimerization to be severely weakened compared to wild-type protein (Table 1). In SPR assays, nectin-1 F129D mutant supported neither homophilic binding of nectin-1 nor heterophilic binding of nectin-3 and nectin-4 (Fig. 1f). An analogous mutation, F136D, in an adhesive D1-2 fragment of mouse nectin-2 also abolished homodimerization in AUC experiments (Table 1). We determined the crystal structure of this mutant, revealing a well-folded protein that does not form the characteristic dimer in the crystal lattice (Supp. Fig. 4). Together, the mutagenesis data suggest that both homo- and heterodimerization of nectin ectodomains in solution depend on the interface observed in crystal structures.

Structural features unique to each nectin dimer interface

While the topology of the homodimer interfaces observed in the nectin ectodomain crystal structures and a number of core interactions are conserved (see above), the nature of some interfacial residues differ between nectins (Fig. 3b, Supp. Fig. 3). These differences potentially account for observed variation in nectin homodimerization affinities. Nectins 1 and 2, which reveal the tightest homophilic binding in AUC (Table 1), bury more hydrophobic surface in their dimer interfaces (734 and 835 $Å^2$, respectively) than nectins 3 and 4 (635 and 680 $Å^2$, respectively), which bind more weakly. The majority of hydrophobic contacts are conserved among nectins and are centered around the Phe docking region, but one residue in the C″ strand is hydrophobic in the tight binders, and hydrophilic in the weak, accounting for much of the observed difference in buried hydrophobic area (Leu90, Pro89, Gln114, Ser90 in nectins 1, 2, 3, and 4, respectively). Differences in hydrophobic contacts are likely to account, at least in part, for stronger homophilic binding of nectins 1 and 2.

While Necl-5 crystallized as a homodimer essentially identical to those of nectins 1–4, there was no measurable homophilic binding in AUC experiments (Table 1) indicating that Necl-5 can accommodate the conserved homodimer geometry, but with very weak affinity.

Interestingly, no strongly unfavorable electrostatic interaction is found at the Necl-5 homodimer interface, and the F-strand residue that is charged in other nectins is Leu in Necl-5 (Leu124, Fig. 3b). However, very few favorable interactions are found in this interface and total buried hydrophobic surface is than in other nectin homodimers (619Å^2). This difference arises primarily from polar residues in the C′ strand and C′C″ loop of Necl-5 that are hydrophobic in other nectins with (Fig. 3b and Supp. Fig 3). These include Ser87, which is hydrophobic in nectins 1 and 2, and Glu82, which has hydrophobic or partially hydrophobic character in all other nectins and closely interacts with the docked Phe residue (Fig. 3b, Supp. Fig. 3). Limited hydrophobic interactions at the homophilic interface are likely to be a major factor underlying both the absence of Necl-5 homophilic binding and weak homophilic binding of nectin-3 and nectin-4.

The structurally-identified dimer mediates *trans* adhesion

Geometrically, the conserved nectin homodimer observed in crystal structures could in principle represent either a *cis* or a *trans* interaction. However, since this is the only interface observed in all five nectin family member structures reported here, and in previous structures of nectin-1[20, 34], human nectin-2 D1[35] and Necl-5 D1-2[36], and since mutation of the interface abolishes nectin binding (Fig. 1, Table 1), the most parsimonious interpretation is that it directly mediates adhesive *trans* interactions.

In order to determine experimentally whether the structurally-observed homodimer interface mediates *trans* interactions under physiological conditions, we assessed binding of full-length nectin-2 in transfected A431D cells via immunofluorescence and chemical cross-linking. The α splice isoform of mouse nectin-2, with a cytoplasmic flag-mCherry tag(Fig. 4a), localized exclusively at cell-cell contacts of transfected A431D cells in a pattern that was indistinguishable from endogenous nectin-2 in these cells (Fig. 4b). A point mutation, F136D, which inactivated nectin-2 dimerization in biophysical and structural experiments (Fig. 1, Table 1, Supp. Fig. 4), severely diminished recruitment of the mutant nectin to cell contacts without affecting localization of endogenous nectin-2, showing the dimerization interface we observe in crystal structures to be essential for recruitment of nectin to cell-cell contacts (Fig. 4b). We then used targeted cross-linking to detect formation on the cell surface of the dimer interface observed in crystal structures. Based on the structure of the homodimer, single cysteine substitutions were introduced at three positions in the D1 domain of mouse nectin-2 to allow crosslinking of the specific dimer configuration at cell junctions using sulfhydryl-reactive cross-linkers: S83C in the C′C″ loop near the apex of the dimer; L72C in the C strand near the base of the dimer and, as a negative control, T49C in the B strand far from the dimerization interface (Fig. 4c). Distances between mutant cysteines in homodimers of S83C and L72C mutants were chosen to match short 1,8-bis(maleimido)diethylene glycol (BM(PEG)$_2$) (14.7Å) and long BM(PEG)$_3$ (17.8Å) cross-linkers, respectively. Subcellular localization of all cysteine mutants was identical to wild-type protein, showing that the mutations did not affect nectin binding (Supp. Fig. 5).

We first examined whether the nectin dimer could be specifically detected using this method. Cells expressing the cysteine mutants were cross-linked with BM(PEG)$_2$ and BM(PEG)$_3$. Western blotting of the cell lysates using anti-flag antibody clearly showed that

cross-linking led to the formation of high molecular weight adducts corresponding in size to nectin dimers (Fig. 4d). In agreement with structural predictions, L72C and S83C mutants could be efficiently cross-linked whereas the T49C mutant, far from the dimer interface, could not. Furthermore, the long cross-linker $BM(PEG)_3$ was markedly more efficient for the L72C mutant, while the shorter cross-linker was more efficient for the S83C mutant, consistent with their relative distances in the homodimer structure. Thus, our cross-linking assay specifically detects the nectin dimer configuration observed in the crystal structures. To further substantiate this conclusion, we introduced the F136D mutation into the S83C mutant. As expected, this double mutant could not be cross-linked into dimers (Fig. 4d).

Specific cross-linking using differentially tagged nectin-2 allowed us to determine the *cis* or *trans* orientation of the dimer at cell contacts. Cells expressing nectin-2 L72C mutant tagged with Flag-mCherry were co-cultured with cells expressing the same mutant tagged instead with Myc-mCherry (Fig. 4a). The co-culture was cross-linked with $BM(PEG)_3$ and cross-linked cells were lysed with 0.5% SDS-containing buffer to completely disrupt non-covalent protein-protein interactions while leaving covalent cross-linked interactions intact. Flag-tagged nectin-2 L72C was then precipitated with anti-Flag antibody. Western blotting of the resulting precipitates using anti-myc antibody clearly showed a cross-linked dimer incorporating both the myc and flag forms of nectin-2 L72C (Fig. 4e). This complex can form only due to specific crosslinking of the nectin dimer in the *trans* orientation between apposed cells expressing myc and flag forms. Our targeted crosslinking experiments thus provide direct evidence that the crystallographically observed dimer common to all nectin structures reported here can form in the *trans* orientation between nectins on apposed cell surfaces. These observations, together with our biophysical, structural and mutagenesis studies strongly support the identification of this interface as the adhesive binding site of nectins.

DISCUSSION

Biophysical, structural and biochemical experiments presented here identify a canonical *trans* adhesive interface that mediates intercellular adhesion between nectins. This dimer, present in all six unrelated crystal lattices reported here, has dimensions and orientation compatible with a cell-to-cell *trans* orientation at adhesive junctions (Fig. 2). Distances between C-termini for full ectodomain dimer structures of nectin-1, nectin-3 and Necl-5 range from 160Å–228Å (Fig. 2), owing to subtype-dependent variations in interdomain angles and dimer angles (Supp. Fig. 6). Assuming an extended conformation for membrane-proximal stalk regions present in full-length nectins, but absent from the crystallized constructs, predicted intermembrane distances are approximately 244 Å, 268Å, and 265Å for nectins 1, 3 and Necl-5, compatible with intermembrane spacings of 150–300Å observed by electron microscopy of adherens junctions[13].

We note that the *trans* binding interface that we identify here could additionally form in a *cis* orientation between nectins that are not engaged in adhesion. Indeed, a cross-linking study by Narita *et al*[20], showed that mutations targeting the same interface could partially inhibit formation of putative nectin-1 *cis* dimers on the surface of dissociated cells. It is currently unclear whether potential formation of the nectin adhesive interface in *cis* plays

any physiologically relevant role. For cadherins, their rigid calcium-bound ectodomain structures geometrically prevent adhesive binding from ectodomains presented on the same cell surface. Relaxation of cadherin rigidity by removal of calcium allows *cis* dimers to form via the adhesive interface[37]. Nectins could rely on similar structural principles to favor *trans* over *cis* binding.

The adhesive dimer described here is the only interface conserved in all six crystal lattices of wild-type nectins. The absence of other conserved interfaces across multiple structures indirectly argues against a physiological role for other ectodomain-mediated interactions between nectins. A potential *cis* dimer interface between parallel D2 domains observed in a previous crystal structure of nectin-1[38] was not observed in our nectin-1 structure nor was an analogous interface observed for other nectins, suggesting that this did not represent a biologically relevant interface. Our six structures fail to reveal any other common interfaces – including any that could geometrically function to cluster nectins in *cis*. Thus, nectin clustering at cell junctions is unlikely to be driven by direct nectin-nectin ectodomain interactions.

Atomic-level basis for nectin adhesive specificity

The crystal structures reported here depict homophilic adhesive interfaces, but mutagenesis data suggest that heterophilic adhesive interactions utilize the same interface region (Fig. 1;[20]). In light of this and the high structural similarity among nectins, analysis of nectin homodimer interfaces, for which all structures are now available, can reveal the molecular basis of heterophilic specificity. Note that in this analysis, sequence numbering refers to human nectins to restrict the analysis of specificity to a single species.

Tight heterophilic binding between cognate nectin pairs (nectin 1+3, nectin 1+4 and nectin 2+3; Fig. 1) likely arises primarily from compatibility with respect to electrostatic interactions. As described above, a potential repulsive electrostatic interaction is observed in homodimers of nectins 1–4 between charged residues in the F-strand that are symmetrically paired in the dimer (e.g. between paired Glu125 residues in nectin-1, see Fig. b). The charge of the residue at this conserved position defines two subgroups within the nectin family: nectins 1 and 2 in which this charge is negative (Glu125 and Glu141[mouse Glu132], respectively), and nectins 3 and 4 in which the charge is positive (Lys149 and Arg128, respectively). In all tight nectin adhesive heterodimers (nectin 1+3, 1+4, and 2+3) each partner belongs to a different subgroup so these charged residues, which lie at the center of each stereotyped interface, are paired with an opposite charge allowing highly favorable salt-bridges to form (Fig. 5a). This is in contrast to homodimers where identical paired charges are expected to repel (Supp. Fig. 3). Additionally, interface maps in which putative heterodimers are modeled on homodimer structures suggest that large hydrophobic contacts form at these heterophilic interfaces (Fig. 5a). Together, charge compatibility and buried hydrophobic surface areas provide a simple explanation for the observed inter-subgroup binding preference of nectins.

An exception to this pattern, that nectins 2 and 4 do not bind despite belonging to different charge subgroups, can be explained by properties of their interfacial residues. Modeling of the putative nectin 2+4 heterodimer on homodimer structures (Fig. 5b) reveals a potential

repulsive interaction between positively charged residues in the C′-C″ loops (Lys88 in nectin-2 and Lys85 in nectin-4) that is likely to destabilize the dimer (Fig. 5b). Additionally, hydrophobic residues (Ala143 and Leu67) stabilizing the nectin-2 homodimer, and polar residues (Ser130 and Gln64) stabilizing the nectin-4 homodimer would be mismatched in a heterocomplex (Fig. 5b, dashes).

Heterodimers between members of the same charge subgroup are not observed (Fig. 1, [7, 17, 21, 22]). These heterodimers would include a repulsive electrostatic interaction between F strands (Fig. 5b) as in homodimers (Fig. 3, Supp. Fig 3). Whereas favorable homodimer interactions are likely to overcome this destabilization (see above), such interactions would be absent from intra-subgroup heterodimer pairings due to mismatches in the interface. Between nectins 3 and 4, polar residues in nectin-3 (Thr87, Ser90 and Glu92) would be mismatched with non-polar residues in nectin-4 (Gly63, Ala66 and Ala68, Fig. 5b dashes). Nectins 1 and 2 are similarly mismatched and additional electrostatic repulsion is likely to occur between Lys75 of nectin-1 and Arg151 of nectin-2 in the C′-C″ loop (Fig. 5b).

Binding interactions of Necl-5

Heterophilic interaction between Necl-5 and nectin-3 was observed in SPR, in agreement with previous observations[7, 21, 24]. Notably, binding responses were very weak compared to other heterophilic interactions (Fig 1,[7, 21, 24]). Weak heterophilic binding of Necl-5, like its weak homophilic binding, likely results from low hydrophobic buried surface area in the dimer due to the lack of hydrophobic residues in the Phe acceptor pocket (Fig 5a). Specificity for nectin-3 may be due hydrophobic interactions near the center of the interface between Leu124 in Necl-5 and Val151 in nectin-3 (Fig. 5a).

Adhesive binding strengths of nectins

Homophilic and heterophilic binding affinities of nectins may be important for understanding their role in morphogenesis. Strong homophilic binding of nectin-1 and nectin-2 (Table 1) suggests potential homophilic roles *in vivo*, but these have not yet been defined, likely because phenotypes related to homophilic adhesion may be masked by functional redundancy between nectin subtypes in knockout studies[10, 25–27].

The quantitative relationship between homophilic and heterophilic binding affinities of nectins remains unclear due to unique problems for quantitation of heterophilic binding affinities in SPR for molecules that bind homophilically and heterophilically through the same interface (see above; [32, 33]). Previous nectin SPR studies would have also been subject to the same technical difficulties that lead to artifacts in determination of heterophilic binding constants. Additionally, reported nanomolar K_D values for nectin-1+3 heterodimerization[7, 22] were derived from assays using nectins artificially dimerized through fusion to IgFc or alkaline phosphatase expression tags[39], which would be expected to lead to apparent K_Ds substantially lower than the true monovalent interactions[40, 41]. Nevertheless, results of our semi-quantitative SPR analysis (Fig. 1) support previous findings showing heterophilic binding interactions to be stronger than homophilic interactions[7, 17, 20–23] and

are consistent with suggested roles for nectins in driving cell sorting processes through differential adhesion[10].

Binding modes in the wider nectin family

Structures of nectin-like proteins Necl-1[42] and Necl-3 [43], which belong to synCAM subgroup[6], each revealed prototypical homodimeric structures that deviate in topology from nectin homodimers described here. Both form through the CC′C″ FG sheet of D1, as is common in Ig superfamily adhesion molecules[44–46], but characteristic Phe docking seen for nectins is not observed in the nectin-like homodimers[42, 43]. Notably, a recent crystal structure of a heterocomplex between Necl-5 D1 and T-cell-Ig-and-ITIM-domain (TIGIT) protein[47] showed a dimer interface remarkably similar to the homodimer interface observed here, despite substantial sequence divergence between TIGIT and nectins. The scope of biologically-relevant interactions mediated between nectins and other proteins through this interface remains to be fully determined.

ONLINE METHODS

Protein expression and purification

cDNA sequences encoding native signal peptides and extracellular regions (D1-D3) of human nectin-1 (Met1-Pro337), -2 (Met1-Pro350), -3 (Met1-Pro359, splice form 1), -4 (Met1-Gln336) and Necl-5 (Met1-Pro334); mouse nectin-1 (Met1-Pro337), -2 (Met1-Pro341, splice-form α), -3 (Met1-Thr401, splice-form α) and -4 (Met1-Gly338); and D1-2 fragments of mouse nectin-2 (Met1-Tyr250) and human nectin-4 (Met1-Ser243) followed by a C-terminal hexahistidine-tag were inserted between HindIII and NotI sites of mammalian expression vector pCEP4 (Invitrogen). The mouse nectin-3 construct included additional residues following the D3 domain comprising part of the ‘stalk’ region between D3 and transmembrane region; all other constructs omit the stalks. Point mutations F129D in human nectin-1 D1-3 and F136D in mouse nectin-2 D1-2 were introduced using the Quikchange method (Stratagene). We introduced constructs into HEK-293F cells using Lipofectamine 2000 (Invitrogen) and maintained transfectants under continuous selection with hygromycin-B (Mediatech). Secreted His-tagged nectins were collected from four liters of conditioned media by Ni-NTA affinity chromatography in a batch procedure (3 hours, 25°C), and were further purified by anion and cation exchange and size exclusion chromatography using an Akta FPLC system (GE Healthcare). Pure proteins were concentrated to 5–15mg/ml in 150mM NaCl, 10mM Tris-Cl pH 8.0 except for nectin-4 proteins for which the NaCl concentration was 50mM, and D1-2 fragments for which Tris-Cl buffer was replaced with 20mM Bis-tris pH 6.0.

Sedimentation equilibrium analytical ultracentrifugation

AUC equilibrium experiments were performed at 25°C, using a Beckman XL-A/I ultracentrifuge with a Ti60An rotor. Data was collected using UV absorbance at 280 nm. Proteins were analyzed immediately following purification to avoid freeze-thaw cycles. Samples were dialyzed in 150 mM NaCl, 10mM Tris-Cl, pH 8.0 for 16 hours at 4°C and 120μL aliquots of sample diluted to 16, 11 and 5.5mM and, additionally, three buffer references were loaded into six-channel equilibrium cells with parallel sides and sapphire

windows. Samples were spun at 12,280*g* for 20 hours, after which four scans were collected (one per hour). Speed was increased to 18,600*g* for ten hours, then to 26,230g for ten hours and to 35,170*g* with four hourly scans taken after each period. The protocol yields a total of 16 scans per protein concentration (48 scans total). Each experiment was reproduced at least twice. We processed and analyzed data using HeteroAnalysis 1.1.44 software (http://www.biotech.uconn.edu/auf) and calculated buffer density and protein v-bars with SednTerp (Alliance Protein Laboratories) software. Data for all concentrations and speeds were fit globally using nonlinear regression to either a monomer-homodimer equilibrium or ideal monomer model.

SPR binding assays

Binding assays were performed using a Biacore T100 biosensor equipped with a Series S NTA chip (GE Healthcare). Nectins were diluted in HBS (HEPES-buffered saline, 10mM HEPES, pH 7.4, 150mM NaCl) to 10μg/mL and immobilized in HBS at 35°C using a modified his-tag/amine coupling protocol, which is described elsewhere [48]. Nectins were immobilized at 200–900 RU which correspond to approximately 40 μM of free monomer for nectins-1, -3, -4 and Necl-5 as calculated using their homophilic equilibrium binding K_D (Table 1, [32]). Nectin-2 was immobilized at lower monomer concentration (6.0μM) since its low homophilic K_D would necessitate unattainably high densities to achieve 40μM monomer. Similar immobilization densities were used for heterophilic and homophilic binding assays.

Nectin analyte binding assays were performed at 25°C in a buffer of 10mM Tris-HCl, pH 8.0, 150 mM NaCl, 1mM EDTA, 0.2 mg/mL BSA and 0.005% Tween 20 (v/v). For the heterophilic experiments, each nectin was diluted in running buffer at a concentration of 12 μM and tested in duplicate. Samples were injected at 50 μL/min for 30s, followed by a 60-second dissociation phase and a 60-second buffer wash at the same flow rate. Following the dissociation phase, binding signals returned to baseline, making surface regeneration unnecessary. Buffer injections were performed between analyte injections for double referencing of binding responses. Data were processed and analyzed using Scrubber 2.0 (BioLogic Software).

For homophilic binding assays, nectins-1, -2, -3 and -4 were tested at 116-0.05μM, 96.8-0.756μM, 44.0-0.18μM and 60.0-0.25μM, respectively. Protein concentration series for nectins 1, 3 and 4 were prepared in running buffer using a three-fold dilution series and a two-fold dilution series for nectin-2. Binding was tested under similar conditions to the heterophilic binding assays, with the exception of a longer (40s) association phase. Analytes were tested in duplicate in order of increasing concentration.

Crystallization and structure determination

Crystals were grown using the vapor diffusion method with 1–2μl hanging drops at 20°C. Crystallization conditions were: 1.8M sodium formate, 0.1M sodium citrate pH5.4, 15% 2*R*, 3*R*-butanediol (cryoprotectant, added before freezing) for human nectin-1 D1-3; 6% (w/v) PEG 6000, 0.05M cadmium sulfate, 0.2M sodium acetate, 0.1M MES pH6.0 with 15% 2*R*, 3*R*-butanediol cryoprotectant for crystal form 1 and 13% (w/v) PEG 3350, 0.42M sodium

isothiocyanate, 0.1M MES pH6.0 with 15% 2*R*, 3*R*-butanediol cryoprotectant for crystal form 2 of mouse nectin-2 D1-2; 1M lithium sulfate, 0.6M ammonium sulfate, 0.1M tri-sodium citrate pH5.5 with 30% (v/v) glycerol cryoprotectant for mouse nectin-2 F136D mutant; 4.6M ammonium acetate, 0.1M sodium acetate pH4.6 with no additional cryoprotectant for human nectin-3 D1-3; 3M NaCl, 0.1M bis-tris pH5.5 with 30% (w/v) D-trehalose cryoprotectant for human nectin-4 D1-2; and 55% (v/v) tacsimate (Hampton Research), 0.1M bicine pH9.0 with an additional 10% (v/v) tacsimate as cryoprotectant for human Necl-5 D1-3.

Data was collected from single crystals at 100K using a wavelength of 0.979Å at the Northeastern Collaborative Access Team beamline 24-ID-E at the Advanced Photon Source, Argonne National Laboratory, Argonne, Illinois, USA (for human nectin-1 D1-3 and human nectin-4 D1-2) and at the X4A and X4C beamlines of the National Synchrotron Light Source, Brookhaven National Laboratory (all other crystals). Data were processed using HKL2000[49]. Structures were solved by molecular replacement using Phaser[50] with human nectin-1 (3ALP, [20]), or regions thereof, as a search model for all structures except human Necl-5 D1-3, for which Necl-5 D1-2 (3EOW, [36]) was used. Structures were refined by iterative rounds of model building in Coot[51] and automated refinement using Refmac[52] with TLS. NCS restraints were used in the refinements of human nectin-1 and-4, mouse nectin-2 form 2. Ramachandran plot statstics (% favored/allowed/disallowed) were: 96.1/3.9/0 (nectin-1), 94.5/5.5/0 (nectin-2 form 1), 95.9/4.1/0 (nectin-2 form 2), 89.7/10.3/0 (nectin-3), 95.9/4.1/0 (nectin-4), 94.4/5.6/0 (Necl-5). Data collection and refinement statistics are listed in Table 2. Crystals of F136D mutant of mouse nectin-2 D1-2, belonging to space group $P6_522$ (a=b=59.9Å, c=210.1Å) diffracted x-rays to 3.25Å with I/σ(I) of 14.2 (3.6 in highest resolution shell), completeness of 99.2% (93.2) and R_{sym} of 0.12 (0.35). The structure was solved by molecular replacement with Phaser[52] using wild-type nectin-2 (form 1) as search model, locating a single molecule in the asymmetric unit (solvent content 46%) with a translation function Z-score of 17.1. 1701 protein and 50 carbohydrate atoms were refined using restrained refinement in refmac against 3967 unique reflections. A single round of refinement yielded a partially refined structure with R_{work}/R_{free} of 23.7/33.6% that is shown in Supp. Fig. 4. Since this was a mutant structure determined only to assess whether the binding interface was ablated, further refinement was not performed.

Cell culture, cross-linking, and immunoprecipitation experiments

Transfection, growth, and immunofluorescence microscopy of human A-431D cells were performed as described elsewhere[53]. The plasmid pRc-mN2 encoding the α splice-form of mouse nectin-2 was constructed by inserting the coding cDNA into pRc-CMV between Hind III and Xba I sites. 1x myc-mCherry or 1x flag-mCherry tags were inserted between Pro513 and Ser514 (see Fig. 4a). Nectin transfectants expressing equal, moderate levels of transgenes were sorted by flow cytometry and used for experiments.

The following antibodies were used: mouse anti-humannectin-2 (clone B-C12, Abcam), mouse anti-Flag M2 (Sigma), and rabbit anti-myc (ab9106, Abcam). Homobifunctional sulfhydryl-reactive cross-linker $BM(PEG)_2$ and $BM(PEG)_3$ (Thermo Scientific) were used for cross-linking experiments. In brief, confluent cultures were incubated for 10 min at 4°C

with phosphate buffered saline (PBS) containing 1 mM of cross-linker. Reactions were stopped by PBS containing 10mM dithiothreitol. Cross-linked cells were either solubilized directly in the SDS-gel sample buffer or subjected to immunoprecipitation, for which cells were extracted with IP-SDS buffer (0.5% SDS in 10 mM Tris-HCl, pH 7.4 with 0.5 mM AEBSF). After solubilization, DNA in lysates was broken by 28G Insulin Syringe, and the SDS-concentration was adjusted to 0.1% with standard 1%-Triton-X-100 IP-buffer. Lysates were cleared by centrifugation (14,000*g*) and flag-tagged nectin was precipitated using anti-Flag agarose (Sigma).

Modeling of nectin heterodimers

Models for all heterodimeric pairs of human nectins were built based on homodimer crystal structures. For nectin-2, the human homodimer structure (3r0n) was used in order to restrict the analysis to one species. Orientations of partner molecules in the homodimer were used to position two protomers in the heterodimer by structural alignment. Heterodimer models were minimally refined using constrained minimization in Charmm [54], consisting of 100 minimization steps with the steepest descent algorithm followed by 300 steps with the conjugate gradient algorithm, while Cα-atoms were harmonically restrained to their position with force constraint of 20 kcal.mol^{-1}Å^{-2}.

Supplementary Material

Refer to Web version on PubMed Central for supplementary material.

Acknowledgments

This work has been supported by grants from the National Institutes of Health (AR44016 and AR057992 to S.M.T., R01 GM062270 to L.S.) and from the National Science Foundation (MCB-0918535 to B.H.). Use of the Advanced Photon Source (APS) for data collection on human nectin-1 (D1-D3) and human nectin-4 (D1-D2) at beamline 24-ID-E was supported by the U. S. Department of Energy, Office of Science, Office of Basic Energy Sciences, under Contract No. DE-AC02-06CH11357. X-ray data for all other nectins were acquired at the X4A and X4C beamlines of the National Synchrotron Light Source, Brookhaven National Laboratory (BNL); the beamlines are operated by the New York Structural Biology center. We thank John Schwanof and Randy Abramowitz at BNL and Narayanasami Sukumar at APS for support with synchrotron data collection.

References

1. Ogita H, Takai Y. Nectins and nectin-like molecules: roles in cell adhesion, polarization, movement, and proliferation. IUBMB Life. 2006; 58:334–343. [PubMed: 16754328]
2. Sakisaka T, Takai Y. Biology and pathology of nectins and nectin-like molecules. Curr Opin Cell Biol. 2004; 16:513–521. [PubMed: 15363801]
3. Takai Y, Nakanishi H. Nectin and afadin: novel organizers of intercellular junctions. J Cell Sci. 2003; 116:17–27. [PubMed: 12456712]
4. Morita H, et al. Nectin-2 and N-cadherin interact through extracellular domains and induce apical accumulation of F-actin in apical constriction of Xenopus neural tube morphogenesis. Development. 2010; 137:1315–1325. [PubMed: 20332149]
5. Ikeda W, et al. Afadin: A key molecule essential for structural organization of cell-cell junctions of polarized epithelia during embryogenesis. J Cell Biol. 1999; 146:1117–1132. [PubMed: 10477764]
6. Biederer T. Bioinformatic characterization of the SynCAM family of immunoglobulin-like domain-containing adhesion molecules. Genomics. 2006; 87:139–150. [PubMed: 16311015]

7. Ikeda W, et al. Tage4/Nectin-like molecule-5 heterophilically trans-interacts with cell adhesion molecule Nectin-3 and enhances cell migration. J Biol Chem. 2003; 278:28167–28172. [PubMed: 12740392]
8. Okabe N, et al. Contacts between the commissural axons and the floor plate cells are mediated by nectins. Dev Biol. 2004; 273:244–256. [PubMed: 15328010]
9. Reymond N, et al. DNAM-1 and PVR regulate monocyte migration through endothelial junctions. J Exp Med. 2004; 199:1331–1341. [PubMed: 15136589]
10. Togashi H, et al. Nectins establish a checkerboard-like cellular pattern in the auditory epithelium. Science. 2011; 333:1144–1147. [PubMed: 21798896]
11. Takahashi K, et al. Nectin/PRR: an immunoglobulin-like cell adhesion molecule recruited to cadherin-based adherens junctions through interaction with Afadin, a PDZ domain-containing protein. J Cell Biol. 1999; 145:539–549. [PubMed: 10225955]
12. Satoh-Horikawa K, et al. Nectin-3, a new member of immunoglobulin-like cell adhesion molecules that shows homophilic and heterophilic cell-cell adhesion activities. J Biol Chem. 2000; 275:10291–10299. [PubMed: 10744716]
13. Meng W, Takeichi M. Adherens junction: molecular architecture and regulation. Cold Spring Harb Perspect Biol. 2009; 1:a002899. [PubMed: 20457565]
14. Aoki J, et al. Mouse homolog of poliovirus receptor-related gene 2 product, mPRR2, mediates homophilic cell aggregation. Exp Cell Res. 1997; 235:374–384. [PubMed: 9299162]
15. Lopez M, et al. The human poliovirus receptor related 2 protein is a new hematopoietic/endothelial homophilic adhesion molecule. Blood. 1998; 92:4602–4611. [PubMed: 9845526]
16. Momose Y, et al. Role of the second immunoglobulin-like loop of nectin in cell-cell adhesion. Biochem Biophys Res Commun. 2002; 293:45–49. [PubMed: 12054561]
17. Reymond N, et al. Nectin4/PRR4, a new afadin-associated member of the nectin family that trans-interacts with nectin1/PRR1 through V domain interaction. J Biol Chem. 2001; 276:43205–43215. [PubMed: 11544254]
18. Struyf F, Martinez WM, Spear PG. Mutations in the N-terminal domains of nectin-1 and nectin-2 reveal differences in requirements for entry of various alphaherpesviruses and for nectin-nectin interactions. J Virol. 2002; 76:12940–12950. [PubMed: 12438620]
19. Miyahara M, et al. Interaction of nectin with afadin is necessary for its clustering at cell-cell contact sites but not for its cis dimerization or trans interaction. J Biol Chem. 2000; 275:613–618. [PubMed: 10617658]
20. Narita H, et al. Crystal Structure of the cis-Dimer of Nectin-1: implications for the architecture of cell-cell junctions. J Biol Chem. 2011; 286:12659–12669. [PubMed: 21325282]
21. Fabre S, et al. Prominent role of the Ig-like V domain in trans-interactions of nectins. Nectin3 and nectin 4 bind to the predicted C-C′-C″-D beta-strands of the nectin1 V domain. J Biol Chem. 2002; 277:27006–27013. [PubMed: 12011057]
22. Yasumi M, Shimizu K, Honda T, Takeuchi M, Takai Y. Role of each immunoglobulin-like loop of nectin for its cell-cell adhesion activity. Biochem Biophys Res Commun. 2003; 302:61–66. [PubMed: 12593848]
23. Martinez-Rico C, et al. Separation force measurements reveal different types of modulation of E-cadherin-based adhesion by nectin-1 and -3. J Biol Chem. 2005; 280:4753–4760. [PubMed: 15550395]
24. Mueller S, Wimmer E. Recruitment of nectin-3 to cell-cell junctions through trans-heterophilic interaction with CD155, a vitronectin and poliovirus receptor that localizes to alpha(v)beta3 integrin-containing membrane microdomains. J Biol Chem. 2003; 278:31251–31260. [PubMed: 12759359]
25. Inagaki M, et al. Role of cell adhesion molecule nectin-3 in spermatid development. Genes Cells. 2006; 11:1125–1132. [PubMed: 16923130]
26. Inagaki M, et al. Roles of cell-adhesion molecules nectin 1 and nectin 3 in ciliary body development. Development. 2005; 132:1525–1537. [PubMed: 15728677]
27. Togashi H, et al. Interneurite affinity is regulated by heterophilic nectin interactions in concert with the cadherin machinery. J Cell Biol. 2006; 174:141–151. [PubMed: 16801389]

28. Ozaki-Kuroda K, et al. Nectin couples cell-cell adhesion and the actin scaffold at heterotypic testicular junctions. Curr Biol. 2002; 12:1145–1150. [PubMed: 12121624]
29. Brancati F, et al. Mutations in PVRL4, encoding cell adhesion molecule nectin-4, cause ectodermal dysplasia-syndactyly syndrome. Am J Hum Genet. 2010; 87:265–273. [PubMed: 20691405]
30. Suzuki K, et al. Mutations of PVRL1, encoding a cell-cell adhesion molecule/herpesvirus receptor, in cleft lip/palate-ectodermal dysplasia. Nat Genet. 2000; 25:427–430. [PubMed: 10932188]
31. Krummenacher C, Baribaud I, Sanzo JF, Cohen GH, Eisenberg RJ. Effects of herpes simplex virus on structure and function of nectin-1/HveC. J Virol. 2002; 76:2424–2433. [PubMed: 11836420]
32. Katsamba P, et al. Linking molecular affinity and cellular specificity in cadherin-mediated adhesion. Proc Natl Acad Sci U S A. 2009 In Press.
33. Mavaddat N, et al. Signaling lymphocytic activation molecule (CDw150) is homophilic but self-associates with very low affinity. J Biol Chem. 2000; 275:28100–28109. [PubMed: 10831600]
34. Zhang N, et al. Binding of herpes simplex virus glycoprotein D to nectin-1 exploits host cell adhesion. Nat Commun. 2011; 2:577. [PubMed: 22146396]
35. Liu J, et al. Crystal Structure of Cell Adhesion Molecule Nectin-2/CD112 and Its Binding to Immune Receptor DNAM-1/CD226. J Immunol. 2012; 188:5511–5520. [PubMed: 22547693]
36. Zhang P, et al. Crystal structure of CD155 and electron microscopic studies of its complexes with polioviruses. Proc Natl Acad Sci U S A. 2008; 105:18284–18289. [PubMed: 19011098]
37. Troyanovsky RB, Sokolov E, Troyanovsky SM. Adhesive and lateral E-cadherin dimers are mediated by the same interface. Mol Cell Biol. 2003; 23:7965–7972. [PubMed: 14585958]
38. Di Giovine P, et al. Structure of herpes simplex virus glycoprotein D bound to the human receptor nectin-1. PLoS Pathog. 2011; 7:e1002277. [PubMed: 21980294]
39. Le Du MH, Stigbrand T, Taussig MJ, Menez A, Stura EA. Crystal structure of alkaline phosphatase from human placenta at 1.8 A resolution. Implication for a substrate specificity. J Biol Chem. 2001; 276:9158–9165. [PubMed: 11124260]
40. Lackmann M, et al. Ligand for EPH-related kinase (LERK) 7 is the preferred high affinity ligand for the HEK receptor. J Biol Chem. 1997; 272:16521–16530. [PubMed: 9195962]
41. Pabbisetty KB, et al. Kinetic analysis of the binding of monomeric and dimeric ephrins to Eph receptors: correlation to function in a growth cone collapse assay. Protein Sci. 2007; 16:355–361. [PubMed: 17322526]
42. Dong X, et al. Crystal structure of the V domain of human Nectin-like molecule-1/Syncam3/Tsll1/Igsf4b, a neural tissue-specific immunoglobulin-like cell-cell adhesion molecule. J Biol Chem. 2006; 281:10610–10617. [PubMed: 16467305]
43. Fogel AI, et al. N-glycosylation at the SynCAM (synaptic cell adhesion molecule) immunoglobulin interface modulates synaptic adhesion. J Biol Chem. 2010; 285:34864–34874. [PubMed: 20739279]
44. Jones EY, Davis SJ, Williams AF, Harlos K, Stuart DI. Crystal structure at 2.8 A resolution of a soluble form of the cell adhesion molecule CD2. Nature. 1992; 360:232–239. [PubMed: 1279440]
45. Velikovsky CA, et al. Structure of natural killer receptor 2B4 bound to CD48 reveals basis for heterophilic recognition in signaling lymphocyte activation molecule family. Immunity. 2007; 27:572–584. [PubMed: 17950006]
46. Schwartz JC, Zhang X, Fedorov AA, Nathenson SG, Almo SC. Structural basis for co-stimulation by the human CTLA-4/B7–2 complex. Nature. 2001; 410:604–608. [PubMed: 11279501]
47. Stengel KF, et al. Structure of TIGIT immunoreceptor bound to poliovirus receptor reveals a cell-cell adhesion and signaling mechanism that requires cis-trans receptor clustering. Proc Natl Acad Sci U S A. 2012; 109:5399–5404. [PubMed: 22421438]
48. Koehnke J, et al. Splice form dependence of beta-neurexin/neuroligin binding interactions. Neuron. 2010; 67:61–74. [PubMed: 20624592]
49. Otwinowski Z, Minor W. Processing of X-ray diffraction data collected in oscillation mode. Macromolecular Crystallography, Pt A. 1997; 276:307–326.
50. McCoy AJ, et al. Phaser crystallographic software. J Appl Crystallogr. 2007; 40:658–674. [PubMed: 19461840]

51. Emsley P, Cowtan K. Coot: model-building tools for molecular graphics. Acta Crystallogr D Biol Crystallogr. 2004; 60:2126–2132. [PubMed: 15572765]

52. Murshudov GN, Vagin AA, Dodson EJ. Refinement of macromolecular structures by the maximum-likelihood method. Acta Crystallogr D Biol Crystallogr. 1997; 53:240–255. [PubMed: 15299926]

53. Troyanovsky RB, Laur O, Troyanovsky SM. Stable and unstable cadherin dimers: mechanisms of formation and roles in cell adhesion. Mol Biol Cell. 2007; 18:4343–4352. [PubMed: 17761538]

54. Brooks BR, et al. CHARMM: the biomolecular simulation program. J Comput Chem. 2009; 30:1545–1614. [PubMed: 19444816]

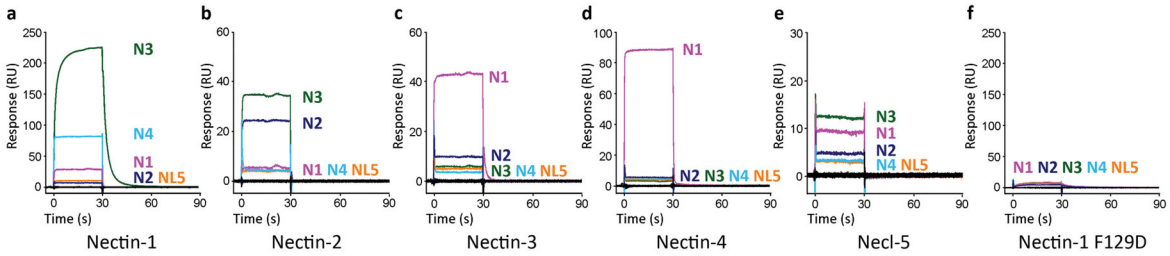

Figure 1. Surface plasmon resonance analysis of nectin binding interactions

SPR chip surfaces were prepared with human D1-3 proteins **(a)** nectin-1, **(b)** nectin-2, **(c)** nectin-3, **(d)** nectin-4, **(e)** Necl-5, and **(f)** nectin-1 F129D mutant. Binding of nectins 1–4 and Necl-5 at 12μM concentration was assessed over each surface. Analyte proteins were continuously injected during the association phase (0–30s) and were replaced with buffer during the dissociation phase (30–90s).

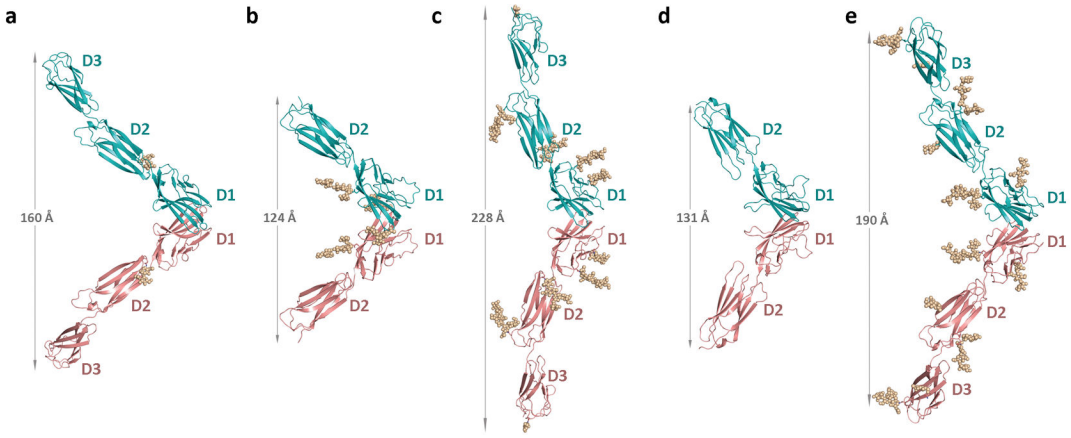

Figure 2. Overall structures of nectin homodimers

Ribbon representations of the homodimer structures of: **(a)** human nectin-1 D1-3, **(b)** mouse nectin-2 D1-2, **(c)** human nectin-3 D1-3, **(d)** human nectin-4 D1-2, and **(e)** human nectin-like 5, all reported here. Individual protomers are colored in blue and salmon. N-linked glycans that were visible in electron density maps are shown as wheat colored spheres. Distances measured between the carboxy termini of partner protomers are shown in grey. In each crystal lattice the depicted homodimers form either between protomers in the crystallographic asymmetric unit (nectin-1) or between symmetry related protomers (all others). Nectin-2 crystallized in two distinct crystal forms each containing similar homodimers; crystal form 1 is depicted in panel **b**.

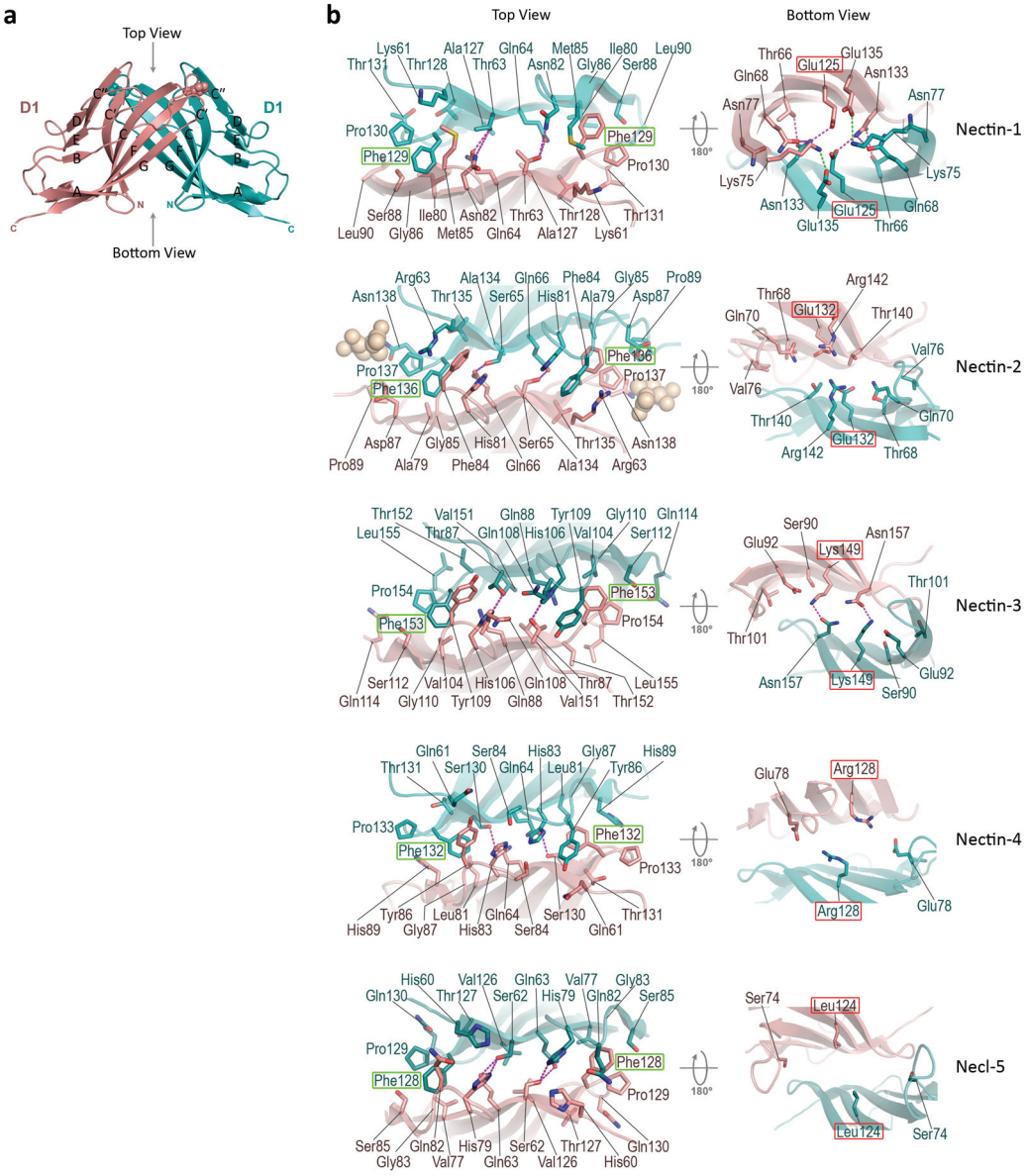

Figure 3. Structural details of nectin homophilic dimers

(a) Ribbon diagram showing the homodimer interface of human nectin-1 D1-3 formed between the CC′C″ FG faces of partner D1 domains. Protomers are colored in blue and salmon. The side chain of Phe129 in the F–G loop, which interacts closely with the partner C′-C″ strands is shown as spheres. **(b)** Structural details of the conserved homodimer interfaces of human nectin-1, mouse nectin-2, human nectin-3, human nectin-4, and human Necl-5. ‘Top View’ and ‘Bottom View’ correspond to the orientations indicated in panel **a**. N-linked glycans close to, but not participating in, the nectin-2 interface are shown as spheres. Side chains of residues that contribute ≥10Å^2 buried surface area in the homodimers are shown as sticks. Intermolecular hydrogen bonds between side chain atoms are shown as magenta dashes and intermolecular salt bridges are shown as green dashes. A highly conserved phenylalanine residue is boxed in green in each interface to aid

comparison. A structurally analogous residue that is charged in nectins 1–4 and symmetrically apposed in each dimer is boxed in red (see main text).

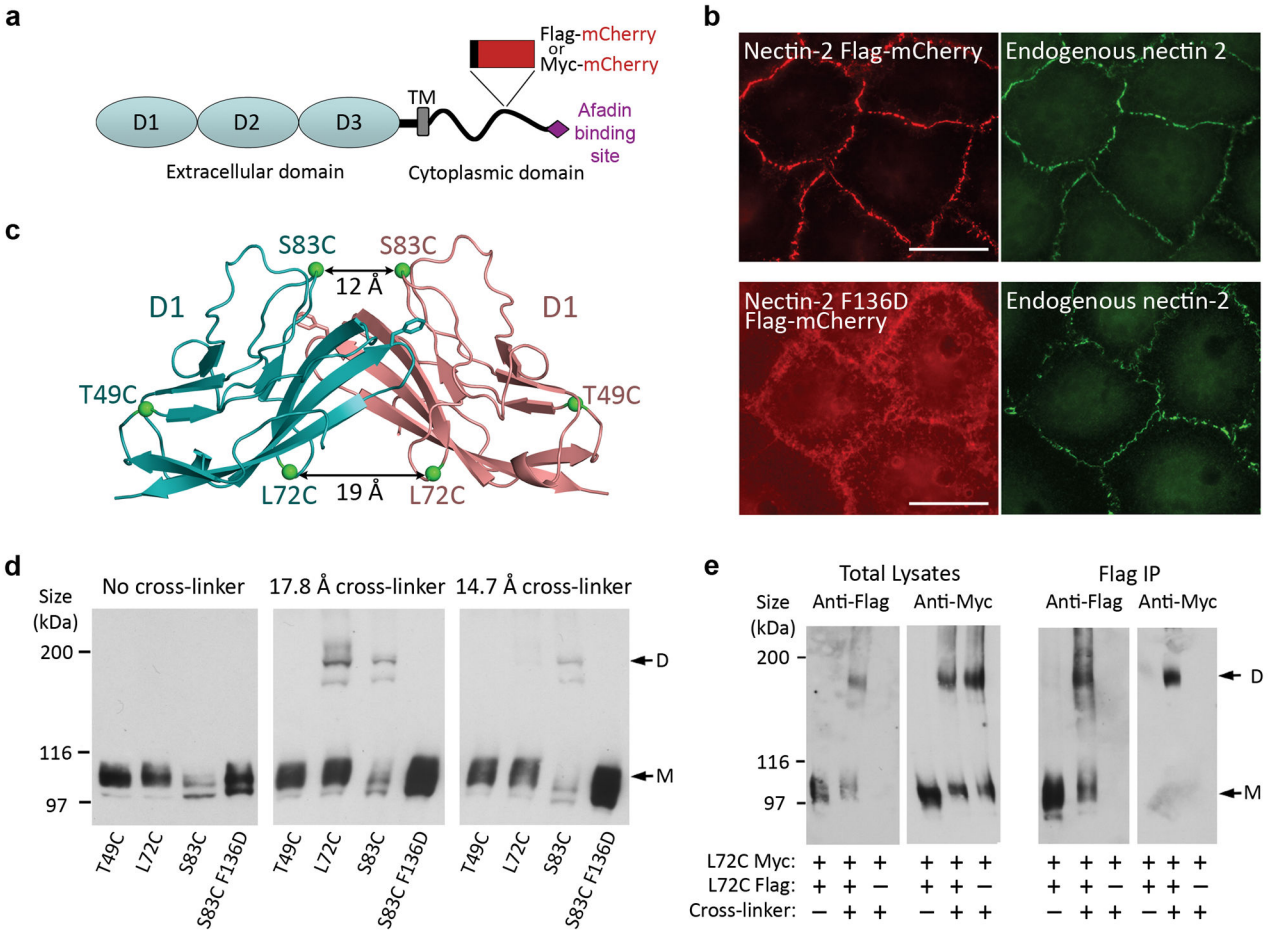

Figure 4. Targeted cross-linking of the nectin homodimer interface in transfected A431D cells

(a) Schematic showing nectin-2 Flag(or Myc)-mCherry constructs used in these studies. Each tag is inserted between residues Pro513 and Ser514 in the nectin-2 cytoplasmic domain, before the afadin binding site. **(b)** Surface localization of wild-type (upper panels) and F136D interface mutant (lower panels) nectin-2 Flag-mCherry in transfected A431D cells. Left panels show red mCherry fluorescence; right panels show FITC immunofluorescence staining for endogenous nectin-2. **(c)** Positions of cysteine substitutions (T49C, L72C, S83C, green spheres) used for targeted cross-linking are shown on a ribbon diagram of the mouse nectin-2 homodimer. L72C and S83C, but not T49C single mutants are predicted to permit cross-linking of the dimer interface. The conserved interface residue Phe136 is shown as sticks. **(d)** Targeted cross-linking of nectin-2 dimers. Reducing SDS-PAGE and anti-Flag Western blot analysis of lysates from confluent cultures of A431D cells expressing T49C, L72C, S83C single mutants or S83C F136D double mutant of nectin-2 Flag-mCherry are shown. Without cross-linking, all mutants migrate as monomer bands of ~100kDa (‘M’, left panel). Cross-linker added to the confluent culture and quenched before lysis stabilizes a dimer form (‘D’, ~200kDa) in L72C and S83C transfectants only (middle and right panels). **(e)** Cross-linking of nectin-2 homodimer interface in a *trans* orientation. A431D cells expressing the Flag tagged form of the L72C mutant were co-cultured with cells expressing a Myc tagged version. After cross-linking,

total cell lysates (left panels) or anti-Flag immunoprecitates (right panels) were separated by reducing SDS-PAGE and blotted against Flag or Myc. In each panel, lane 1 represents Myc-Flag co-cultures without cross-linker; lane 2 represents Myc-Flag co-cultures with crosslinker; lane 3 represents Myc monocultures with cross-linker. *Trans* dimer ('D', right panel) is immunoprecipitated with anti-Flag and blots with anti-Myc antibodies.

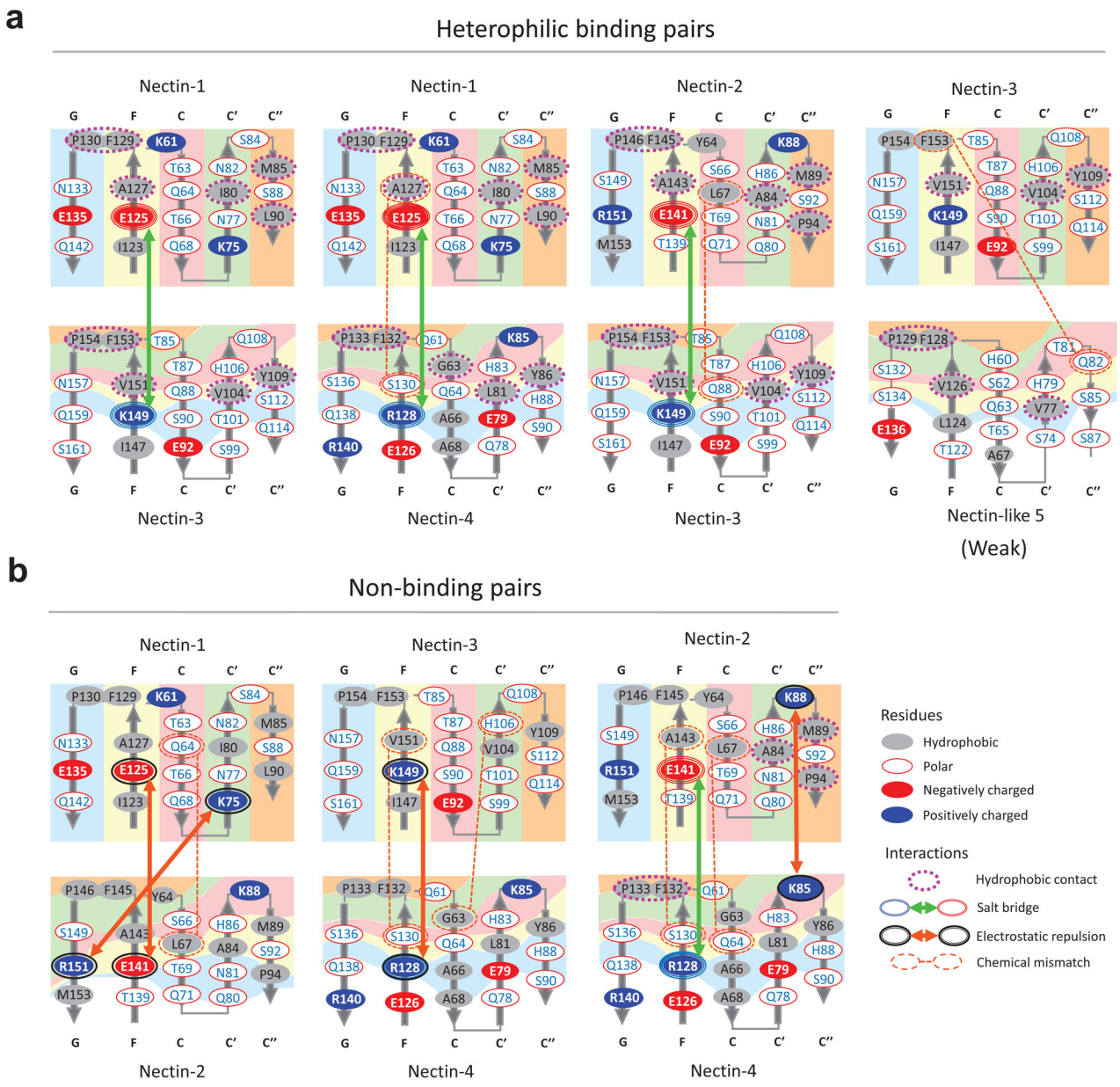

Figure 5. Analysis of the molecular basis of nectin binding specificity

Schematic diagrams of **(a)** heterophilic binding pairs and **(b)** non-binding pairs of human nectins, each modeled on the homophilic crystal structures. β-strands are labeled and shown as arrows. A different colored background denotes each β-strand in the upper panels; in the lower panels these background colors show the position and orientation of the contacting β-strands of the partner molecule. The chemical nature (hydrophobic, polar, charged) of interfacial residues are color coded as defined in the graphical legend. Interactions are denoted by arrows and are also color coded. Residues involved in hydrophobic contacts are surrounded with a brown dashed line. Favorable electrostatic interactions are shown in

green, and unfavorable electrostatic interactions, characteristic of non-binding pairs, are shown in orange. Chemical mismatches between residues are indicated with dashed lines.

Table 1

Analytical ultracentrifugation analysis of nectin homodimerization

Protein	Monomer M_w from mass spec. (kDa)	Apparent M_w in AUC (kDa)	Oligomeric state	K_D dimerization (μM)
Human				
Nectin-1 (D1-D3)	43.3[a]	67.5 ± 0.79[b]	Dimer	17.5 ± 2.2 [b]
Nectin-2 (D1-D3)	39.4	75.8 ± 0.10	Dimer	0.392 ± 0.029
Nectin-3 (D1-D3)	47.5	52.6 ± 0.077	Weak dimer	228 ± 9.5
Nectin-4 (D1-D3)	35.6	43.1 ± 1.2	Weak dimer	153 ± 28
Necl-5 (D1-D3)	46.8	45.7 ± 1.6	Monomer	n.d.[c]
Nectin-1 (D1-D3) F129D	43.6[a]	43.8 ± 0.099	Weak dimer	820 ± 101
Mouse				
Nectin-1 (D1-D3)	44.2	65.3 ± 0.87	Dimer	22.6 ± 1.3
Nectin-2 (D1-D3)	40.2	75.7 ± 0.11	Dimer	1.09 ± 0.10
Nectin-3 (D1-D3)	57.6	66.4 ± 1.2	Weak dimer	122 ± 16
Nectin-4 (D1-D3)	36.1	42.1 ± 2.1	Weak dimer	278 ± 137
Nectin-2 (D1-D2)	28.5	49.1 ± 0.17	Dimer	7.62 ± 0.016
Nectin-2 (D1-D2) F136D	26.4	24.4 ± 0.50	Monomer	n.d.
Heterocomplexes (Human)				
Nectin-1 (D1-D3) + Nectin-3 (D1-D3)	[43.3 + 47.5][d]	86.7 ± 0.08	Dimer	n.d.
Nectin-1 (D1-D3) + Nectin-4 (D1-D3)	[43.3 + 35.6]	77.4 ± 1.0	Dimer	n.d.

[a] Heterogeneous glycosylation of human nectin-1 produces a broad mass distribution (~35–45kDa); mass of the major peak (~80%) is listed

[b] Errors indicate data range from two or more experiments

[c] Not determined

[d] Sum of individual experimental masses.

Table 2

Data collection and refinement statistics

	Nectin-1 D1-3 Human	Nectin-2 D1-2 Mouse *Form 1*	Nectin-2 D1-2 Mouse *Form 2*	Nectin-3 D1-3 Human	Nectin-4 D1-2 Human	Nectin-like 5 D1-3 Human
Data collection						
Space group	$P6_3$	$P3_112$	$P3_121$	$P6_522$	$C222_1$	$P6_522$
Cell dimensions						
a, *b*, *c* (Å)	106.3, 106.3, 334.6	68.8, 68.8, 159.8	117.0, 117.0, 158.5	131.9, 131.9, 247.5	86.0, 142.8, 341.8	139.1, 139.1, 274.0
α, *β*, *γ* (°)	90, 90, 120	90, 90, 120	90, 90, 120	90, 90, 120	90, 90, 90	90, 90, 120
Resolution (Å)	40 - 3.20	40 - 2.54	40 – 3.35	40 – 3.93	20-3.5	40 – 3.60
R_{sym} or R_{merge}	0.10 (0.51) *	0.06 (0.54)	0.09 (0.54)	0.07 (0.61)	0.161 (0.57)	0.11 (0.55)
$I/\sigma I$	14.2 (2.2)	20.5 (3.9)	18.7 (4.0)	24.0 (3.2)	7.8 (2.4)	13.7 (2.5)
Completeness (%)	99.0 (92.4)	99.4 (99.7)	99.2 (99.9)	98.3 (99.1)	99.4 (100.0)	99.8 (99.9)
Redundancy	6.0 (4.8)	6.1 (6.2)	5.6 (5.7)	5.9 (6.1)	5.2 (5.5)	6.3 (5.7)
Refinement						
Resolution (Å)	20 – 3.20	20-2.54	20-3.35	20.0-3.93	20.0-3.50	20-3.60
No. reflections	33108	13414	17484	11139	25299	17564
R_{work}/R_{free}	23.3/25.8	22.1/26.8	24.4/29.0	24.7/27.9	25.7/29.0	24.8/27.3
No. atoms						
Protein	9470	1718	5118	2342	9257	2342
Carbohydrate	112	131	270	243	-	268
Ion	12	4	-	-	-	-
Water	4	36	16	-	-	-
B-factors						
Protein	96.4	84.1	136.1	171.0	93.9	112.6
Carbohydrate	91.7	144.9	165.2	166.7	-	149.7
Ion	50.2	113.4	-	-	-	-
Water	41.8	63.9	50.2	-	-	-
R.m.s. deviations						
Bond lengths (Å)	0.014	0.016	0.013	0.016	0.012	0.014
Bond angles (°)	1.650	1.667	1.548	1.295	1.649	1.761

Author Manuscript

Author Manuscript

Author Manuscript

* Values in parentheses are for highest-resolution shell.